Detecting the dynamical instability of complex time series via partitioned entropy

Kota Shiozawa, Taisuke Uemura, and Isao T. Tokuda*

Graduate School of Science and Engineering, Ritsumeikan University, 1-1-1 Noji-Higashi, Kusatsu, Shiga 525-8577, Japan

(Received 10 August 2022; accepted 15 December 2022; published 11 January 2023)

A method is proposed to detect the dynamical instability of complex time series. We focus on how the partitioned entropy of an initially localized region of the attractor evolves in time and show that its growth rate corresponds to the first Lyapunov exponent. To avoid spurious detection of the dynamical instability, a criterion is further introduced to distinguish chaos from limit cycles or tori. Numerical experiments using prototypical models of chaotic systems demonstrate that the growth rate of the partitioned entropy indeed provides a good estimate of the first Lyapunov exponent. The method is also shown to be robust against observational noise and dynamical noise. Analysis of experimental data measured from a physical model of the vocal folds highlights the practical applicability of the present method to real-world data. Advantages of the present method over conventional methods are also discussed.

DOI: 10.1103/PhysRevE.107.014207

I. INTRODUCTION

Time series analysis is essential for modeling, prediction, and controlling of unknown systems in many scientific and engineering fields [1]. Typically, such systems are nonlinear and the observed time series is complex, which cannot be treated with linear methods alone. To deal with such complex time series, numerous methods have been developed such as machine learning [2–5], complex networks [6–9], and entropy-based techniques [10–14]. In this paper, we focus on the entropy-based techniques, which have been widely applied to quantify the complexity of experimental time series.

As the measure of complexity, various quantities such as the fractal dimension, the Lyapunov exponent, and the Kolmogorov-Sinai (KS) entropy can be computed [15–20]. The fractal dimension characterizes a self-similar geometry of the underlying attractor [15], whereas the Lyapunov exponent measures a divergence rate of nearby trajectories [16–18]. The KS entropy quantifies a growth rate of the entropy required to characterize trajectories and is smaller than or equal to the sum of the positive Lyapunov exponents [20]. Numerous methods have been proposed to estimate the correlation dimension [15], the Lyapunov exponent [16–18], and the KS entropy [19]. These methods work well under an idealistic situation in that the time series is generated from low-dimensional chaos. As soon as the data are contaminated with noise, however, these methods break down and the estimated results become unreliable.

As another approach to estimate the KS entropy, return times of a dynamical system can be also used [21–23]. The return times represent a series of time intervals between two consecutive events, and have been used to characterize the behavior of complex systems [24,25]. Although this approach is quite effective for systems in which the events can be well defined, it is not straightforward to formulate events for unknown systems. In general, real-world systems are governed by unknown equations and the data generated from them are noisy, short, and even nonstationary.

To overcome these difficulties, alternative approaches using the idea of symbolic dynamics have been proposed [26]. The symbolic dynamics approach is based on a coarse-graining of the measured time series. The time series is converted into a symbolic sequence and, as a measure of the complexity, the information entropy [27] is estimated from the probability distribution of the symbols. The advantages of the symbolic dynamics include the computational efficiency and the robustness against noise. Because of these practicalities, the symbolic dynamics methods have been widely used to analyze experimental time series. Kurths *et al.* applied the symbolic dynamics for the analysis of heart rate variability data and found that electrocardiograms of patients with high cardiac risks exhibit a higher level of complexity compared to those of healthy subjects [28]. Costa *et al.* proposed a method to compute multiscale entropy, which takes into account the multiple time scales of a time series, and applied it successfully to complex physiological data [29,30]. Bandt and Pompe proposed a method to compute permutation entropy, which encodes times series of a given length into a ranked order sequence, and showed that their quantity is highly correlated with the Lyapunov exponent [31,32]. Miyano and Gotoda proposed a variation of the permutation entropy and applied it to a time series of flame front location [33]. Despite the usefulness of these complexity measures, it is not straightforward to interpret the obtained results, because the relationship between the complexity measures and the dynamical quantities such as the Lyapunov exponents and the KS entropy is unclear.

Towards developing a complexity measure, which has a clear link to the theory of nonlinear dynamics, Amigó *et al.* found that the growth rate of the permutation entropy is equal to the KS entropy [34]. The growth rate, however, is affected by strong finite-size corrections and thus the KS entropy

*isao@fc.ritsumei.ac.jp

estimated from the permutation entropy was found unreliable [35]. To fix this problem, Politi introduced a correction term that modified the permutation entropy and demonstrated that the modified permutation entropy improves the estimation of the KS entropy [35]. The method, however, is rather weak against noise, since the modified permutation entropy should be computed for at least two settings of the embedding dimensions d and $d+1$. The additional dimension amplifies the noise effect by increasing an inaccurate symbol in the sequence. Because of this reason, an improved method that is capable of computing the complexity measure with a fixed embedding dimension is desirable. Along this line, Shiozawa and Miyano proposed a method that focuses on the time evolution of the permutation entropy with a fixed embedding dimension [36]. They numerically showed that the estimated complexity has a linear correlation with the first Lyapunov exponent. Their method, however, cannot distinguish chaos from periodic data, since high complexity values are estimated even from periodic data. Moreover, the relationship between their complexity measure and the nonlinear dynamic quantities remains unclear.

In this paper, we extend the method of Shiozawa and Miyano to achieve the following properties:

(1) The complexity measure can be computed with a fixed embedding dimension.

(2) The estimated complexity has a clear relationship with the nonlinear dynamic quantity, i.e., the first Lyapunov exponent.

(3) The method is robust against noise and can distinguish complex time series from limit cycles or tori.

To verify the validity of our proposed method, we apply it to various time series data simulated from prototypical models of chaotic systems as well as to experimental data from physical model of the vocal folds. The effect of noise is also examined.

II. THEORETICAL BACKGROUND

This section illustrates how the information entropy of an attractor relates to the dynamical quantity of the underlying system. More specifically, we focus on the entropy of a subset of an attractor, which is initially localized in a same region, and follow its time evolution.

Let us consider an attractor in a d-dimensional phase space and partition it into M cells of size ε. We extract a set of points located inside of the ith cell and consider them as initial conditions, from which the system evolves. As time grows, the set of initial conditions evolves into an ellipsoid-like structure. The longest diameter of the ellipsoid can be approximated as $l_i(t) \approx \varepsilon e^{\lambda_1^i t}$, where λ_1^i is the local first Lyapunov exponent that corresponds to the most rapidly expanding direction near the ith cell (Fig. 1 illustrates the expanded diameter in the case of $d=2$). The minimum number of cells required to cover the stretched ellipsoid at time t is approximated as

$$m_i(t) \approx \frac{l_i(t)}{l_i(0)} \approx e^{\lambda_1^i t}. \tag{1}$$

For simplicity, we assume that the ellipsoid is equally distributed in the $m_i(t)$ cells so that the probability that the system state, initially located in the ith cell, is found in the jth cell at time t is given by

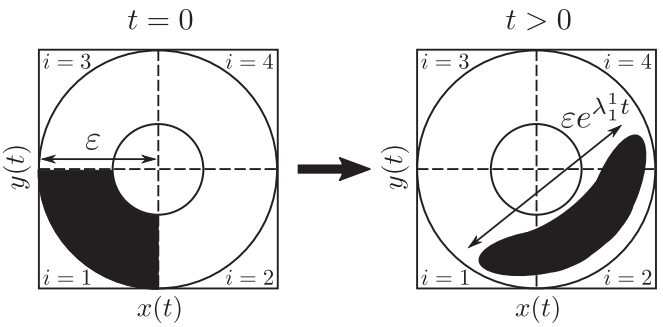

FIG. 1. Illustration of an evolution of partitioned attractor. In two-dimensional space ($d=2$), an attractor exhibits a donut-like structure, which is partitioned into four cells ($M=4$, $i=1,2,3,4$). At time $t=0$, a set of initial conditions is covered by the first cell (shaded area on the left panel). As time t passes, the set of initial states evolves into an ellipsoid (shaded area on the right panel), the diameter of which is expanded to $l_i(t) \approx \varepsilon e^{\lambda_1^i t}$. The number of cells required to cover the stretched ellipsoid can be approximated as $m_i(t) \approx e^{\lambda_1^i t}$.

$$p_{ij}(t) = \frac{1}{m_i(t)}, \tag{2}$$

where $j = 1, \ldots, m_i(t)$. The information entropy $h_i(t)$ of the ellipsoid at time t is thus given as

$$\begin{aligned} h_i(t) &= -\sum_{j=1}^{m_i} p_{ij}(t) \ln p_{ij}(t) \\ &= -\sum_{j=1}^{m_i} \frac{1}{m_i} \ln \frac{1}{m_i} \approx \lambda_1^i t. \end{aligned} \tag{3}$$

Since the first Lyapunov exponent λ_1 of the attractor is given by a spatial averaging of the local first Lyapunov exponents $\{\lambda_1^i\}$, averaging of the information entropy $h_i(t)$ over all cells, which cover all regions of the initial conditions, may yield

$$h(t) = \sum_{i=1}^{M} \rho_i h_i(t) \approx \lambda_1 t, \tag{4}$$

where ρ_i is the probability that the system state falls within the ith cell (i.e., coarse-grained invariant measure of the attractor). We call $h(t)$ "partitioned entropy" because it focuses on the entropy of the states, which are initially partitioned into a same cell. Equation (4) implies that the partitioned entropy $h(t)$ grows linearly in time and its time derivative gives the first Lyapunov exponent λ_1. Note that Eq. (4) holds only for $t \lesssim \lambda_1^{-1}$, since the diameter of the ellipsoid grows rapidly and becomes comparable to the size of the whole attractor at time $t \sim \lambda_1^{-1}$.

III. METHOD

In the previous section, we described the idea of the partitioned entropy of an attractor and showed that its growth rate corresponds to the first Lyapunov exponent. This section presents an efficient and robust method to calculate the partitioned entropy from an observed time series and shows

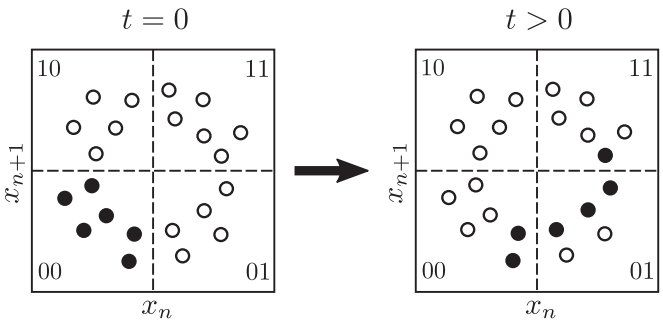

FIG. 2. Time evolution of system states on the reconstructed attractor in a two-dimensional space. The reconstructed attractor is partitioned into four cells (00, 01, 10, 11) by the threshold (dashed lines). The system states (solid circles) located within the cell 00 evolve in time, where the number of cells required to cover the spreading system states increases as time passes.

that its growth rate indeed provides a good estimate for the first Lyapunov exponent.

First, the time series is transformed into a symbolic sequence. Our scheme is based on the attractor reconstruction using the time-delay coordinates [37,38] and binary encoding of the delay coordinate vectors. Consider a time series $\{x_n\} = \{x(nT\Delta t)\}_{n=0}^{N-1}$ composed of N data points with a time interval of $T\Delta t$ (T is an integer to skip the sampling data points and to adjust the time-delay length). We reconstruct the attractor into d-dimensional delay coordinate space as $\mathbf{v}_n = (x_n, x_{n+1}, \ldots, x_{n+d-1})$. The nth system state $\mathbf{v}_n$ in the embedding space is transformed into a sequence of d-bit binary numbers $b_n b_{n+1} \cdots b_{n+d-1}$. For instance, when the embedding dimension is two (i.e., $d = 2$), the nth system state is transformed into two-bit binary numbers as

$$b_n b_{n+1} = \begin{cases} 00 & \text{if } x_n < x_{\text{thres}} \text{ and } x_{n+1} < x_{\text{thres}} \\ 01 & \text{if } x_n < x_{\text{thres}} \text{ and } x_{n+1} \geqslant x_{\text{thres}} \\ 10 & \text{if } x_n \geqslant x_{\text{thres}} \text{ and } x_{n+1} < x_{\text{thres}} \\ 11 & \text{if } x_n \geqslant x_{\text{thres}} \text{ and } x_{n+1} \geqslant x_{\text{thres}}, \end{cases} \tag{5}$$

where x_{thres} represents a threshold, for which the median of $\{x_n\}$ is used so that the binary numbers 0 and 1 appear with an equal probability.

By tracing the time evolution of the system state, the reconstructed attractor $\{\mathbf{v}_n\}$ is transformed into a sequence of d-bit binary numbers $S = \{b_0 b_1 \cdots b_{d-1}, \ldots, b_{N-d} b_{N-d+1} \cdots b_{N-1}\}$. This procedure can be viewed as partitioning the reconstructed attractor into 2^d cells. Figure 2 illustrates the case of $d = 2$, in which the attractor is partitioned into $2^2 = 4$ cells by the threshold x_{thres} (dashed lines) and four symbols 00, 01, 10, and 11 are assigned to the individual cells.

Next, we denote each of the 2^d binary number sequences by a symbol a_i ($i = 1, \ldots, 2^d$) and rewrite the reconstructed attractor as a symbolic sequence $S = \{a_n\}$. By tracing the symbolic sequence of initial conditions in the same cell, the partitioned entropy can be computed at each time step as follows. Suppose, for example, we have the following symbolic sequence:

$$S = \{a_1, a_2, a_4, \ldots, a_1, a_2, a_3, \ldots, a_1, a_4, a_2\}. \tag{6}$$

We pick up all a_1's from the whole sequence S and collect them as a set of initial symbols at time step $\tau = 0$ as

$$S_1(0) = \{a_1, \ldots, a_1, \ldots, a_1\}. \tag{7}$$

In other words, the set $S_1(0)$ corresponds to the set of system states located in the cell, to which the symbol a_1 is assigned. In the next time step $\tau = 1$, the set of the same symbols evolves into

$$S_1(1) = \{a_2, \ldots, a_2, \ldots, a_4\}, \tag{8}$$

where $S_1(1)$ consists of symbols next to a_1 in S. In a similar manner, the set of symbols that evolves from $S_1(1)$ is collected as

$$S_1(2) = \{a_4, \ldots, a_3, \ldots, a_2\}. \tag{9}$$

This procedure is illustrated in Fig. 2, where the states (solid circles on the left panel), initially located in the cell 00, evolve into nearby cells (solid circles on the right panel) in the next step. By repeating this procedure, the time evolution of the set of symbols, which start from a_1, can be created as $S_1(\tau)$ for $\tau \geqslant 0$. The partitioned entropy for $S_1(\tau)$ is computed as

$$h_1(\tau) = -\sum_{j=1}^{2^d} p_{1j}(\tau) \ln p_{1j}(\tau), \tag{10}$$

where $p_{1j}(\tau)$ represents the probability that the symbol a_1 evolves into a_j after τ steps. Note that $h_1(0) = 0$, since $S_1(0)$ consists only of a_1. Another note is that the dimension of time t is recovered as $h_1(t) = h_1(\tau T\Delta t)$.

So far, we focused only on the time evolution of the set of symbols starting from a_1. The same computation can be performed to obtain i th partitioned entropy $h_i(t)$ for $S_i(\tau)$ that starts from a_i ($i = 1, \ldots, 2^d$). Finally, the partitioned entropy $h(t)$ for the whole attractor is obtained by taking the weighted average of $\{h_i(t)\}_{i=1}^{2^d}$ as

$$h(t) = \sum_{i=1}^{2^d} \rho_i h_i(t). \tag{11}$$

As before, the weights $\{\rho_i\}$ correspond to the coarse-grained density of the attractor. According to Eq. (4), the time derivative of the partitioned entropy $h(t)$ should yield the first Lyapunov exponent λ_1.

Figure 3(a) shows a typical behavior of the partitioned entropy computed from a time series generated from the Rössler equations in a chaotic regime (details described in the next section). The partitioned entropy increases linearly in time and saturates around $t = 18$, where the system states, initially localized within a single cell, spread over the whole attractor. To estimate the slope, which provides an approximate value of the first Lyapunov exponent, we fit the function $\hat{h}(t) = \min(\alpha t, \beta)$ to the entropy curve using the least-squares method. Among the fitted parameters α and β, α determines the slope of the linear region, which approximates the first Lyapunov exponent.

Figure 3(b), on the other hand, shows the case that the partitioned entropy was calculated from a time series in a limit cycle regime. Although the first Lyapunov exponent should be zero for the limit cycle, the partitioned entropy increases rapidly in the initial phase, giving rise to a positive slope

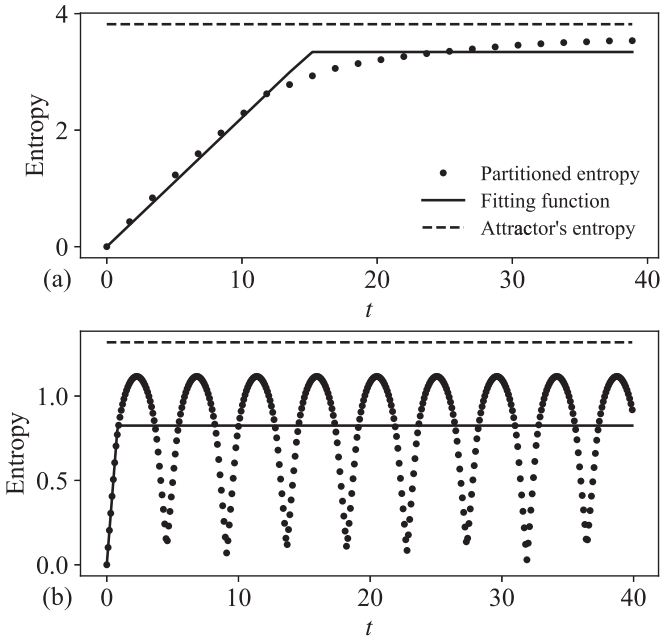

FIG. 3. Time evolution of the partitioned entropy $h(t)$ in the case of (a) chaos and (b) limit cycle. The partitioned entropy is calculated from the y variable of the Rössler equations (14) with $a = 0.55$, $b = 2$, and $c = 4$ for chaos and $a = 0.505$, $b = 2$, and $c = 4$ for limit cycle. The time series consist of $N = 3 \times 10^5$ data points and the embedding dimension is set to $d = 7$. The solid line represents a fitting function $\hat{h} = \min(\alpha t, \beta)$, whereas the dashed line represents the entropy of the whole attractor, $h_{\max}$.

α. This behavior is due to a coarse-graining effect. As time grows, the set of system states started from a localized region of the limit cycle remains localized in the state space but can occupy multiple cells when crossing the partitions. Such a temporal spreading of the localized states into multiple cells may increase the entropy and forms a positive slope. To avoid such a spurious detection of the positive Lyapunov exponent, we distinguish chaos from limit cycles in the following manner. In the case of chaos, the set of initially localized states may eventually spread over the attractor and its distribution converges to the probability density of the whole attractor, i.e., $\{\rho_i\}$. This implies that, as time grows, the partitioned entropy $h(t)$ converges to the entropy of the whole attractor, i.e., $h_{\max} = -\sum_{i=1}^{2^d} \rho_i \ln \rho_i$. On the other hand, in the case of limit cycles, the states remain localized and do not spread. Thus, the partitioned entropy $h(t)$ may not converge to $h_{\max}$.

As a quantity to distinguish chaos from limit cycles, the mean partitioned entropy is introduced as

$$h_{\text{mean}} = \lim_{t\to\infty} \frac{1}{t} \int_0^t h(t')dt'. \tag{12}$$

In the case of chaos, the ratio between the mean entropy and the attractor's entropy should be close to one (i.e., $h_{\text{mean}}/h_{\max} \approx 1$). In the case of limit cycles, this ratio should be much smaller than one (i.e., $h_{\text{mean}}/h_{\max} < 1$). Note that, since Eq. (12) converges slowly, it is convenient to calculate the average of $h(t)$ over a time interval of $t_1 \leqslant t \leqslant t_2$, where t_1 and t_2 are set to be large enough. By introducing a threshold r, the time series can be considered chaotic if $h_{\text{mean}}/h_{\max} \geqslant r$ and periodic otherwise. Finally, the first Lyapunov exponent is estimated as

$$\gamma = \begin{cases} \alpha & \text{if } h_{\text{mean}}/h_{\max} \geqslant r \\ 0 & \text{if } h_{\text{mean}}/h_{\max} < r. \end{cases} \tag{13}$$

IV. NUMERICAL EXPERIMENTS

In this section, we examine the performance of our method through numerical experiments. As the target systems, the Rössler system [39] and the Langford system [40] were utilized. The Rössler system is described by

$$\dot{x} = -y - z, \quad \dot{y} = x + ay, \quad \dot{z} = b + z(x - c). \tag{14}$$

The parameter values were fixed as $b = 2$ and $c = 4$, whereas the bifurcation parameter a was varied as $0.45 \leqslant a \leqslant 0.55$ with an increment of $\Delta a = 10^{-4}$. As the time series, the y variable was observed. The Langford system, on the other hand, is described by

$$\begin{aligned} \dot{x} &= (z - \beta)x - \omega y, \quad \dot{y} = \omega x + (z - \beta)y, \\ \dot{z} &= \lambda + \alpha z - \frac{z^3}{3} - (x^2 - y^2)(1 + \rho z) + \varepsilon z x^3, \end{aligned} \tag{15}$$

where the bifurcation parameter ε was varied as $0 \leqslant \varepsilon \leqslant 0.25$ with an increment of $\Delta\varepsilon = 5 \times 10^{-3}$ and the other parameters were fixed as $\alpha = 1$, $\beta = 0.7$, $\lambda = 0.6$, $\omega = 3.5$, and $\rho = 0.25$. As the time series, the z variable was observed. The two systems were numerically integrated using the fourth-order Runge-Kutta algorithm with a time step of $\Delta t = 0.01$. All time series data were generated with $N = 3 \times 10^5$ data points after a transient period was removed. The skipping time T was chosen in such a way that the time delay $T\Delta t$ gives the first minimum of the mutual information [41]. The embedding dimension, the time interval to compute the mean partitioned entropy, and the threshold value were set to $d = 7$, $t_1 = 200$, $t_2 = 300$, and $r = 0.8$, respectively.

Figure 4 shows the results obtained for the Rössler system. The first Lyapunov exponent γ estimated by the present method in Fig. 4(a) is compared with the true exponent λ_1 computed by the Shimada-Nagashima algorithm [42]. To clarify the relationship between γ and λ_1, a linear regression, $\gamma = c_0 + c_1\lambda_1 + \epsilon$ (ϵ represents the regression error), was introduced. The intercept c_0, the slope c_1, the correlation coefficient R, and the coefficient of determination, R^2, are summarized in Table I. The high correlation between the two values (correlation coefficient $R = 0.96$) implies that the growth rate of the partitioned entropy, defined by Eq. (4), provides a good estimate of the first Lyapunov exponent. Our method also successfully detected the existence domains of limit cycles (i.e., periodic windows), including the ones around $a \approx 0.459, 0.505$. As shown in Fig. 4(b), the ratio between the mean entropy and the attractor's entropy, $h_{\text{mean}}/h_{\max}$, became smaller than the threshold $r = 0.8$ (dashed line) in these periodic windows.

As shown in Fig. 5, comparable results were obtained for the Langford system. The first Lyapunov exponent γ estimated by the present method was in a good agreement with the true value λ_1 [Fig. 5(a)]. The correlation coefficient be-

TABLE I. Relationship between γ and λ_1 quantified by correlation coefficient R, linear regression ($\gamma = c_0 + c_1\lambda_1 + \epsilon$), and coefficient of determination, R^2.

System	Intercept, c_0	Slope, c_1	Correlation coefficient, R	Coefficient of determination, R^2
Rössler	0.0016	1.28	0.96	0.92
Langford	−0.0052	0.89	0.94	0.88

tween the two values was $R = 0.94$. The periodic windows were precisely detected in Fig. 5(b). Moreover, the Langford system generated quasiperiodic oscillations for $\varepsilon \leqslant 0.025$, which have been correctly identified with the zero Lyapunov exponent $\gamma = 0$. Thus, our method is also capable of distinguishing chaos from tori.

Next, we study the effect of observational noise. As the original time series, the y variable was collected from the Rössler system. To generate chaotic time series, the parameters were set to $a = 0.55$, $b = 2$, and $c = 4$, whereas they were set to $a = 0.2$, $b = 0.2$, and $c = 2$ to generate periodic time series. Then, the observational noise was added as $y + \xi$, where ξ is a zero-mean *Gaussian* white noise $N(0, \sigma_{\text{obs}}^2)$. The noise strength was set to $0 \leqslant \sigma_{\text{obs}} \leqslant 0.256$ for the chaotic time series and $0 \leqslant \sigma_{\text{obs}} \leqslant 0.224$ for the periodic time series, where the maximum noise strength was set to 10% of the standard deviation of the noise-free time series. As shown in Fig. 6, our method was quite robust against observational noise added to the chaotic time series. As the noise intensity was increased, the estimated first Lyapunov exponent γ remained closely located to the true value λ_1 [Fig. 6(a)]. As shown in Fig. 6(b), the ratio between the mean entropy and the attractor's entropy, $h_{\text{mean}}/h_{\text{max}}$, was consistently above the threshold $r = 0.8$ (dashed line), indicating that the system is chaotic. Similar results were obtained also for the periodic time series [Fig. 6(c)]. Even if the noise intensity was increased, the first Lyapunov exponent γ was constantly estimated to be zero and the ratio between the mean entropy and the attractor's entropy, $h_{\text{mean}}/h_{\text{max}}$, was below the threshold $r = 0.8$. Compared to the noise-free condition, this ratio dropped [Fig. 6(d)] because the noise broadened the distribution of the limit cycle in the state space and increased its entropy h_{max}. Despite this effect, our method worked reasonably well for both chaotic and limit cycle data in the presence of the observational noise.

We also considered the effect of dynamical noise. Since chaotic attractors could easily lose their stability even by a small amount of dynamical noise, we considered only the case of a limit cycle. A dynamical noise term was added to the Rössler system as $\dot{x} = -y - z + \eta$, $\dot{y} = x + ay$,

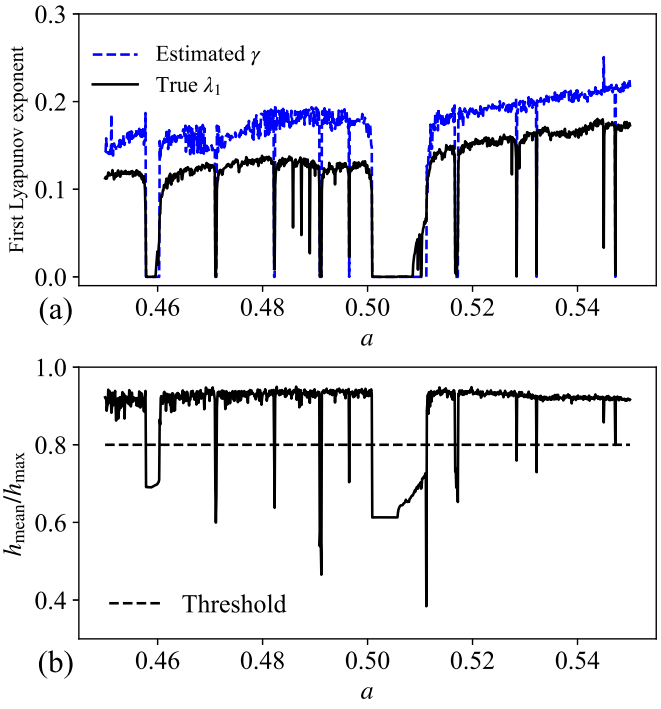

FIG. 4. Rössler system with a varying bifurcation parameter $a \in [0.45, 0.55]$. (a) True value of the first Lyapunov exponent λ_1 calculated by the Shimada-Nagashima algorithm and estimate of the first Lyapunov exponent γ obtained by the present method. (b) Ratio between the mean entropy and the attractor's entropy, $h_{\text{mean}}/h_{\text{max}}$. The dashed line indicates the threshold $r = 0.8$, above which the system is considered chaotic.

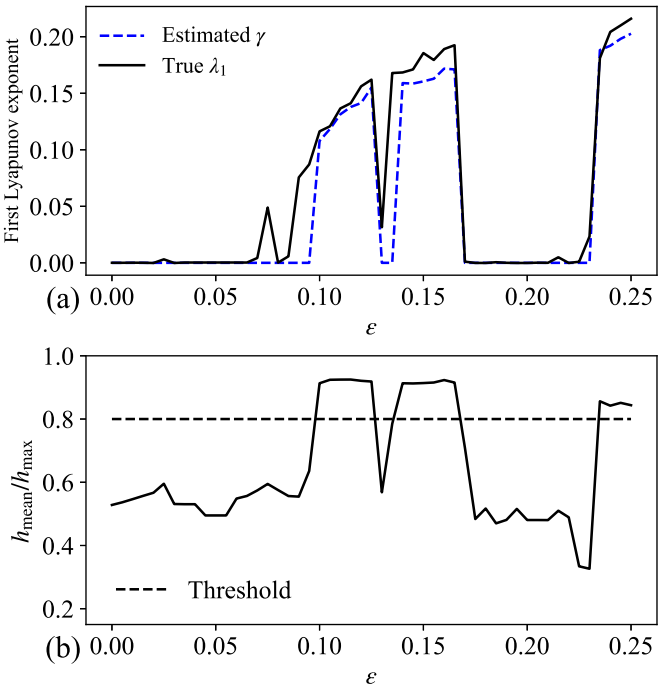

FIG. 5. Langford system with a varying bifurcation parameter $\varepsilon \in [0, 0.25]$. (a) True value of the first Lyapunov exponent λ_1 calculated by the Shimada-Nagashima algorithm and estimate of the first Lyapunov exponent γ obtained by the present method. (b) Ratio between the mean entropy and the attractor's entropy, $h_{\text{mean}}/h_{\text{max}}$. The dashed line indicates the threshold $r = 0.8$, above which the system is considered chaotic.

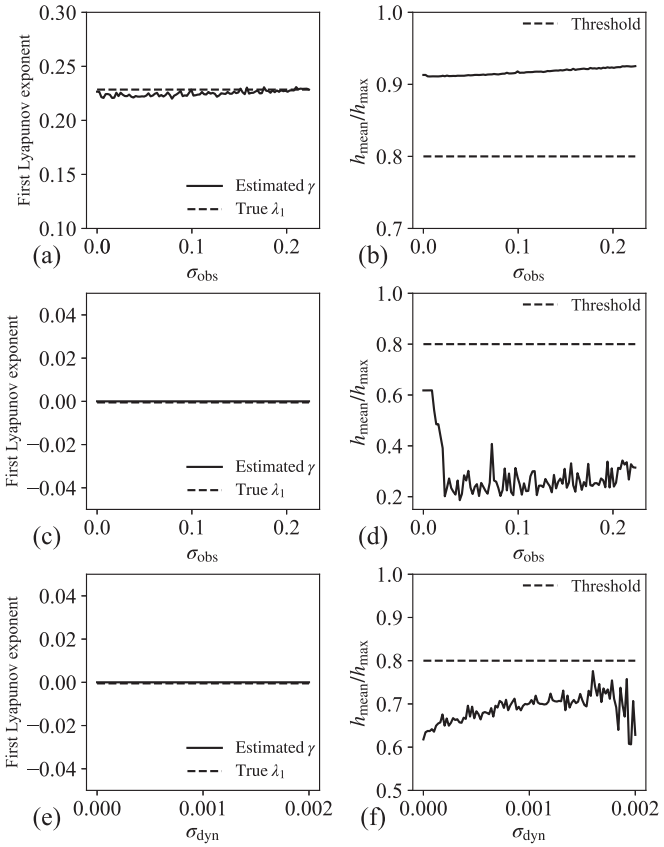

FIG. 6. Effects of noise added to the Rössler system. Observational noise is added to both [(a), (b)] chaotic and [(c), (d)] periodic time series, whereas [(e), (f)] dynamical noise is added to a periodic time series. In (a), (c), and (e), dependence of the estimated Lyapunov exponent γ (solid line) and the true value λ_1 (dotted line) on the noise intensity is shown. In (b), (e), and (f), the ratio between the mean entropy and the attractor's entropy, $h_{\mathrm{mean}}/h_{\mathrm{max}}$, is drawn as a function of the noise intensity.

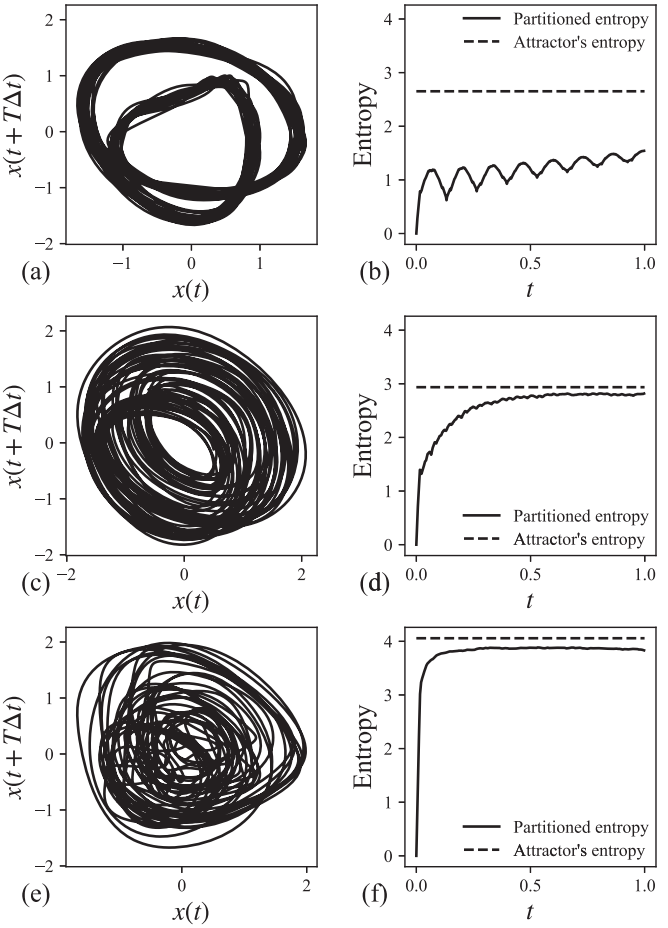

FIG. 7. Application to experimental data from silicone model of the vocal folds. [(a), (c), (e)] Reconstructed attractors and [(b), (d), (f)] the time evolution of the partitioned entropy for #3P-a-2-1, #3P-a-3-2, and #3P-c-3-2, respectively.

$\dot{z} = b + z(x - c)$, where η represents a *Gaussian* white noise (i.e., $\langle \eta(t) \rangle = 0$, $\langle \eta(t)\eta(s) \rangle = \sigma_{\mathrm{dyn}}^2 \delta(t - s)$). The parameter values were set to $a = 0.2$, $b = 0.2$, and $c = 2$, and the noise intensity was varied as $0 \leqslant \sigma_{\mathrm{dyn}} \leqslant 0.002$. The stochastic differential equations were numerically integrated by the Euler-Maruyama method [43] with a time step of $\Delta t = 0.01$. As the time series, the y variable was observed. As shown in Fig. 6(e), our method was robust also against dynamical noise. As the noise intensity was increased, the ratio between the mean entropy and the attractor's entropy, $h_{\mathrm{mean}}/h_{\mathrm{max}}$, increased gradually [Fig. 6(f)], because the initially localized limit cycle attractor spread into other regions by the dynamical noise. Although this effect makes it a more delicate procedure to distinguish noisy limit cycles from chaos, our method correctly identified periodic structure in the time series.

V. APPLICATION TO EXPERIMENTAL DATA

To examine the practical applicability of the present method to real-world data, experimental data were measured from a physical model of the vocal folds. The physical model, called the "magnetic resonance imaging (MRI) model," has been constructed based on a geometry scanned from a magnetic resonance image of a human larynx. It has been widely utilized to understand the mechanism of vocal fold oscillations in human voice production [44]. In this setup, a vocal fold polyp was attached to one side of the vocal fold to produce asymmetry in their oscillations. Such asymmetry is known to cause chaos and tori in vocal fold oscillations [45]. The experimental setup to realize flow-induced oscillations of the vocal fold model is detailed in [46]. As the time series, subglottal pressure (i.e., pressure of the airflow below the glottis) was measured by a pressure transducer and recorded with a sampling time interval of $\Delta t = 8 \times 10^{-5}$ s. Three sets of time series (#3P-a-2-1, #3P-a-3-2, and #3P-c-3-2), each of which consists of $N = 1.2 \times 10^5$ data points, were collected. To reduce nonstationary effect and high-frequency noise, a bandpass filter with a passband from 70 to 500 Hz was applied. The skipping time T was chosen in such a way that the time delay $T\,\Delta t$ gave the first minimum of the mutual information [41]. The embedding dimension, the time interval to compute the mean entropy, and the threshold value were set to $d = 7$, $t_1 = 0.5$ s, $t_2 = 1$ s, and $r = 0.8$, respectively. Figure 7 shows the reconstructed attractors and the time evolution of the partitioned entropy calculated from the time series. As shown in Fig. 7(a), the first data set (#3P-a-2-1) draws a limit-

TABLE II. The estimated Lyapunov exponents γ and the ratio between the mean entropy and the attractor's entropy, $h_{\mathrm{mean}}/h_{\mathrm{max}}$, obtained from the analysis of experimental data (#3P-a-2-1, #3P-a-3-2, #3P-c-3-2).

Data	γ (s^{-1})	$h_{\mathrm{mean}}/h_{\mathrm{max}}$
#3P-a-2-1	0	0.50
#3P-a-3-2	25.1	0.95
#3P-c-3-2	183.9	0.95

cycle-like attractor. The corresponding partitioned entropy exhibited an oscillatory behavior and did not reach h_{max}, implying that the time series is periodic [Fig. 7(b)]. The second data set (#3P-a-3-2), on the other hand, displayed an attractor resembling a chaotic torus [Fig. 7(c)]. The power spectrum of the time series gave rise to two peaks at 80 and 130 Hz, which dominated the chaotic behavior. The corresponding partitioned entropy increased as time grows and converged to h_{max}, implying that the time series is chaotic [Fig. 7(d)]. The third data set (#3P-c-3-2) showed a more complex attractor than the second data set [Fig. 7(e)]. The corresponding partitioned entropy increased more rapidly and saturated quickly, implying that the time series is again chaotic [Fig. 7(f)].

Note that, in Figs. 7(d) and 7(f), the partitioned entropy $h(t)$ saturated but did not reach the attractor's entropy h_{max}. This might come from the fact that only a part of the whole data points (i.e., N_i out of N) is used to compute the individual partitioned entropy $h_i(t)$. The reduced data points may give rise to a lower complexity compared to the one computed from the whole data set.

In Table II, the estimated values of the Lyapunov exponent γ and the ratios between the mean entropy and the attractor's entropy, $h_{\mathrm{mean}}/h_{\mathrm{max}}$, are summarized for the three data sets. The ratio was below the threshold value ($r = 0.8$) for the first data set (#3P-a-2-1), whereas it was above the threshold for the second and third data sets (#3P-a-3-2 and #3P-c-3-2). This confirms that the first data set represents a limit cycle dynamics, whereas the second and third data sets are chaotic. The Lyapunov exponent γ estimated for the third data set was much larger than that for the second data set. This is also consistent with our view that the attractors reconstructed from the second and third data sets represent a weakly chaotic torus and a fully developed chaos, respectively.

VI. DISCUSSIONS AND CONCLUSIONS

In this paper, we have proposed a method to quantify the complexity of a time series. We focused on how the partitioned entropy of an initially localized region of the attractor evolves in time and showed that its growth rate corresponds to the first Lyapunov exponent. Numerical experiments using the prototypical models of chaos (i.e., Rössler and Langford systems) demonstrated that the growth rate of the partitioned entropy indeed provided a good estimate of the Lyapunov exponent. In the case that the system has only a single positive Lyapunov exponent, this provides an estimate for the KS entropy. Our numerical experiments also showed that the method is robust against observational noise and dynamical noise. Analysis of experimental data measured from a physical model of the vocal folds further demonstrated the practical applicability of the present method to real-world data.

We have shown that our method provides a good estimate for the first Lyapunov exponent. It should be noted, however, that there is a gap between the estimated and true values. Namely, our method overestimated the first Lyapunov exponent of the Rössler system in Fig. 4. We consider that this might be due to a coarse-graining effect. As time t evolves, the data points, which were initially localized within a same cell, may split into more cells than expected when they were crossing the cellular borders. This would overall increase the partitioned entropy and consequently overestimate the complexity of the attractor. The coarse-graining effect should depend upon the system dynamics as well as the attractor geometry, since such overestimation was not observed in the Langford system in Fig. 5.

To discuss the dependence of our approach on the partitioning scheme, the present study employed the binary partition to extract the symbolic dynamics. There could be various ways to partition the data such as the Bandt-Pompe partition [31]. Although the Bandt-Pompe partition is defined based on a ranking order of the consecutive time points, it divides the embedding space into static nonoverlapping regions in a similar manner as the present binary partition [36,47]. It should be noted, however, that the binary partition is more suitable for our method, because we can set a relatively large embedding dimension d compared to the Bandt-Pompe partition. While the number of the cells is 2^d for the binary partition, it is $d!$ for the Bandt-Pompe partition. Such a rapid increase in the number of cells with an increasing embedding dimension makes it computationally more challenging, to estimate the attractor entropy. Another note on the binary partition is that it does not satisfy the conditions of the generating Markov partition, which exactly preserves invariant properties of the dynamical system [48]. Although such a mathematically rigorous approach has clear advantages (e.g., the symbolic sequence contains all essential information of the underlying dynamics and can be treated as independent random sources), finding such a Markov partition is nontrivial for general dynamical systems, especially for experimental data, whose dynamics is unknown. For the sake of practicality, the present study utilized the binary partition, which has been shown effective for measuring the complexity of dynamical systems including experimental data [33,49].

Compared to the preceding methods that simply utilized the information entropy of a symbolic dynamics to quantify the complexity of time series [28–33], the present approach has an advantage that the partitioned entropy is clearly related to dynamical quantity (i.e., the first Lyapunov exponent and the KS entropy) of the underlying system, which enables straightforward interpretation of the obtained results. Some studies such as the method of Politi [35] clarified that the growth rate of his modified permutation entropy corresponds to the KS entropy. His method, however, is rather weak against noise, because the modified permutation entropy should be calculated for multiple settings of the embedding dimension, e.g., d and $d + 1$. Such an additional embedding dimension increases the risk that incorrect symbols are assigned to the symbolic sequence due to noise, which is inevitable in real-world systems. In contrast, our method works only with a

single embedding dimension, which enables robust estimation of the first Lyapunov exponent even in the presence of noise. Moreover, Politi's method requires *a priori* knowledge on the fractal dimension of the attractor, whereas our method does not require such knowledge.

As a means to estimate the Lyapunov exponent, the present approach also has several advantages. Unlike conventional methods, which typically trace nearby trajectories of the reconstructed attractor and detect an exponential increase in their distances [16–18], our method converts the time series into a symbolic sequence and traces its time evolution. Such a coarse-grained approach is robust against noise and greatly reduces the computational cost.

Our coarse-grained approach is related to the methods of estimating the KS entropy based on the return times [21–23]. The return times measure how much time it takes for a data point to make two consecutive returns to a given region and their distribution can be used to estimate the KS entropy. Our method, on the other hand, utilizes a spatial distribution of the data points to compute the KS entropy. Although the distributions of the two quantities may not be exactly the same, they can be closely related to each other, since both of them contain enough information on the KS entropy of the underlying dynamics. The relationship between our method and the return times should be addressed in a future study. We also note that our approach can be related to the hitting times [50] as well as the recurrence plots [51], since these two notions are intimately linked to the return times [52,53].

Finally, an interesting question is to ask how our approach is extended to hyperchaotic systems. In the present study, we have shown that, in the case that the system has only one positive Lyapunov exponent, the growth rate of the partitioned entropy is determined by the first Lyapunov exponent, which is equivalent to the KS entropy. For hyperchaotic systems which have multiple positive Lyapunov exponents, it is unclear whether the growth rate is still governed by the KS entropy. Such an issue will be addressed in our future study.

ACKNOWLEDGMENTS

This work was partially supported by the Grant-in-Aid for Scientific Research (Grants No. 19H01002 and No. 20K11875) from the Japan Society for the Promotion of Science (JSPS). K.S. was supported by JST, the establishment of university fellowships towards the creation of science technology innovation (Grant No. JPMJFS2146).

[1] H. Kantz and T. Schreiber, *Nonlinear Time Series Analysis*, Vol. 7 (Cambridge University Press, Cambridge, U.K., 2004).

[2] S. L. Brunton, J. L. Proctor, and J. N. Kutz, Discovering governing equations from data by sparse identification of nonlinear dynamical systems, Proc. Natl. Acad. Sci. USA. **113**, 3932 (2016).

[3] J. Pathak, B. Hunt, M. Girvan, Z. Lu, and E. Ott, Model-Free Prediction of Large Spatiotemporally Chaotic Systems from Data: A Reservoir Computing Approach, Phys. Rev. Lett. **120**, 024102 (2018).

[4] H. Ismail Fawaz, G. Forestier, J. Weber, L. Idoumghar, and P.-A. Muller, Deep learning for time series classification: A review, Data Min. Knowl. Disc. **33**, 917 (2019).

[5] A. Tealab, Time series forecasting using artificial neural networks methodologies: A systematic review, Future Comput. Inf. J. **3**, 334 (2018).

[6] J. Zhang and M. Small, Complex Network from Pseudoperiodic Time Series: Topology Versus Dynamics, Phys. Rev. Lett. **96**, 238701 (2006).

[7] L. Lacasa, B. Luque, F. Ballesteros, J. Luque, and J. C. Nuno, From time series to complex networks: The visibility graph, Proc. Natl. Acad. Sci. U.S.A. **105**, 4972 (2008).

[8] N. Marwan, J. F. Donges, Y. Zou, R. V. Donner, and J. Kurths, Complex network approach for recurrence analysis of time series, Phys. Lett. A **373**, 4246 (2009).

[9] Y. Zou, R. V. Donner, N. Marwan, J. F. Donges, and J. Kurths, Complex network approaches to nonlinear time series analysis, Phys. Rep. **787**, 1 (2019).

[10] D. Toker, F. T. Sommer, and M. D'Esposito, A simple method for detecting chaos in nature, Commun. Biol. **3**, 11 (2020).

[11] M. Staniek and K. Lehnertz, Symbolic Transfer Entropy, Phys. Rev. Lett. **100**, 158101 (2008).

[12] Y. Li, S. Wang, Y. Yang, and Z. Deng, Multiscale symbolic fuzzy entropy: An entropy denoising method for weak feature extraction of rotating machinery, Mech. Syst. Signal Process. **162**, 108052 (2022).

[13] S. Chen, P. Shang, and Y. Wu, Weighted multiscale Rényi permutation entropy of nonlinear time series, Physica A **496**, 548 (2018).

[14] C. S. Daw, C. E. A. Finney, and E. R. Tracy, A review of symbolic analysis of experimental data, Rev. Sci. Instrum. **74**, 915 (2003).

[15] P. Grassberger and I. Procaccia, Characterization of Strange Attractors, Phys. Rev. Lett. **50**, 346 (1983).

[16] A. Wolf, J. B. Swift, H. L. Swinney, and J. A. Vastano, Determining Lyapunov exponents from a time series, Physica D **16**, 285 (1985).

[17] M. T. Rosenstein, J. J. Collins, and C. J. De Luca, A practical method for calculating largest Lyapunov exponents from small data sets, Physica D **65**, 117 (1993).

[18] H. Kantz, A robust method to estimate the maximal Lyapunov exponent of a time series, Phys. Lett. A **185**, 77 (1994).

[19] P. Grassberger and I. Procaccia, Estimation of the Kolmogorov entropy from a chaotic signal, Phys. Rev. A **28**, 2591 (1983).

[20] J.-P. Eckmann and D. Ruelle, Ergodic theory of chaos and strange attractors, in *The Theory of Chaotic Attractors* (Springer, Berlin, 1985), pp. 273–312.

[21] M. S. Baptista, D. M. Maranhão, and J. C. Sartorelli, Dynamical estimates of chaotic systems from Poincaré recurrences, Chaos **19**, 043115 (2009).

[22] P. R. Pinto, M. S. Baptista, and I. S. Labouriau, Density of first Poincaré returns, periodic orbits, and Kolmogorov-Sinai entropy, Commun. Nonlinear Sci. Numer. Simul. **16**, 863 (2011).

[23] M. S. Baptista, E. J. Ngamga, P. R. Pinto, M. Brito, and J. Kurths, Kolmogorov-Sinai entropy from recurrence times, Phys. Lett. A **374**, 1135 (2010).
[24] F. T. Arecchi, A. Lapucci, R. Meucci, J. A. Roversi, and P. H. Coullet, Experimental characterization of Shil'nikov chaos by statistics of return times, Europhys. Lett. **6**, 677 (1988).
[25] Z. d. O. Guimarães-Filho, I. L. Caldas, R. Viana, J. Kurths, I. C. Nascimento, and Y. K. Kuznetsov, Recurrence quantification analysis of electrostatic fluctuations in fusion plasmas, Phys. Lett. A **372**, 1088 (2008).
[26] J. Kurths, U. Schwarz, A. Witt, R. T. Krampe, and M. Abel, Measures of complexity in signal analysis, AIP Conf. Proc. **375**, 33 (1996).
[27] C. E. Shannon, Communication theory of secrecy systems, Bell Syst. Tech. J. **28**, 656 (1949).
[28] J. Kurths, A. Voss, P. Saparin, A. Witt, H. Kleiner, and N. Wessel, Quantitative analysis of heart rate variability, Chaos **5**, 88 (1995).
[29] M. Costa, A. L. Goldberger, and C.-K. Peng, Multiscale Entropy Analysis of Complex Physiologic Time Series, Phys. Rev. Lett. **89**, 068102 (2002).
[30] M. Costa, A. L. Goldberger, and C.-K. Peng, Multiscale entropy analysis of biological signals, Phys. Rev. E **71**, 021906 (2005).
[31] C. Bandt and B. Pompe, Permutation Entropy: A Natural Complexity Measure for Time Series, Phys. Rev. Lett. **88**, 174102 (2002).
[32] C. Bandt, G. Keller, and B. Pompe, Entropy of interval maps via permutations, Nonlinearity **15**, 1595 (2002).
[33] T. Miyano and H. Gotoda, Estimation of the degree of dynamical instability from the information entropy of symbolic dynamics, Phys. Rev. E **96**, 042203 (2017).
[34] J. M. Amigó, M. B. Kennel, and L. Kocarev, The permutation entropy rate equals the metric entropy rate for ergodic information sources and ergodic dynamical systems, Physica D **210**, 77 (2005).
[35] A. Politi, Quantifying the Dynamical Complexity of Chaotic Time Series, Phys. Rev. Lett. **118**, 144101 (2017).
[36] K. Shiozawa and T. Miyano, Symbolic diffusion entropy rate of chaotic time series as a surrogate measure for the largest Lyapunov exponent, Phys. Rev. E **100**, 032221 (2019).
[37] F. Takens, Detecting strange attractors in turbulence, in *Dynamical Systems and Turbulence, Warwick 1980* (Springer, Berlin, 1981), pp. 366–381.
[38] T. Sauer, J. A. Yorke, and M. Casdagli, Embedology, J. Stat. Phys. **65**, 579 (1991).
[39] O. E. Rössler, An equation for continuous chaos, Phys. Lett. A **57**, 397 (1976).
[40] W. F. Langford, Numerical studies of torus bifurcations, in *Numerical Methods for Bifurcation Problems* (Springer, Berlin, 1984), pp. 285–295.
[41] A. M. Fraser and H. L. Swinney, Independent coordinates for strange attractors from mutual information, Phys. Rev. A **33**, 1134 (1986).
[42] I. Shimada and T. Nagashima, A numerical approach to ergodic problem of dissipative dynamical systems, Prog. Theor. Phys. **61**, 1605 (1979).
[43] G. Maruyama, Continuous Markov processes and stochastic equations, Rend. Circolo Mat. Palermo **4**, 48 (1955).
[44] B. A. Pickup and S. L. Thomson, Flow-induced vibratory response of idealized versus magnetic resonance imaging-based synthetic vocal fold models, J. Acoust. Soc. Am. **128**, EL124 (2010).
[45] I. Steinecke and H. Herzel, Bifurcations in an asymmetric vocal-fold model, J. Acoust. Soc. Am. **97**, 1874 (1995).
[46] K. Migimatsu and I. T. Tokuda, Experimental study on nonlinear source-filter interaction using synthetic vocal fold models, J. Acoust. Soc. Am. **146**, 983 (2019).
[47] I. Stolz and K. Keller, A general symbolic approach to Kolmogorov-Sinai entropy, Entropy **19**, 675 (2017).
[48] N. Rubido, C. Grebogi, and M. S. Baptista, Entropy-based generating Markov partitions for complex systems, Chaos **28**, 033611 (2018).
[49] K. Karamanos, A. Peratzakis, P. Kapiris, S. Nikolopoulos, J. Kopanas, and K. Eftaxias, Extracting preseismic electromagnetic signatures in terms of symbolic dynamics, Nonlinear Process. Geophys. **12**, 835 (2005).
[50] M. Kac, On the notion of recurrence in discrete stochastic processes, Bull. Am. Math. Soc. **53**, 1002 (1947).
[51] J.-P. Eckmann, S. O. Kamphorst, and D. Ruelle, Recurrence plots of dynamical systems, Europhys. Lett. **4**, 973 (1987).
[52] N. Haydn, Y. Lacroix, and S. Vaienti, Hitting and return times in ergodic dynamical systems, Ann. Probab. **33**, 2043 (2005).
[53] C. Letellier, Estimating the Shannon Entropy: Recurrence Plots Versus Symbolic Dynamics, Phys. Rev. Lett. **96**, 254102 (2006).